

Article

Crotonaldehyde Adsorption on Cu-Pt Surface Alloys: A Quantum Mechanics Study

Ricardo Ruvalcaba ¹, Jonathan Guerrero-Sanchez ¹, Noboru Takeuchi ¹ and Francisco Zaera ^{2,*} 

¹ Centro de Nanociencias y Nanotecnología, Universidad Nacional Autónoma de México, Ensenada 22860, Baja California, Mexico

² Department of Chemistry and UCR Center for Catalysis, University of California Riverside, Riverside, CA 9252, USA

* Correspondence: zaera@ucr.edu

Abstract: The adsorption of crotonaldehyde on Cu-Pt alloy surfaces was characterized by density functional theory (DFT). Two surfaces were considered: Cu₂Pt/Cu(111) and Cu₃Pt/Cu(111). It was determined that the presence of Pt on the surface, even when isolated as single atoms fully surrounded by Cu, provides additional stability for the adsorbates, increasing the magnitude of the adsorption energy by as much as 40 kJ/mol. The preferred bonding on both surfaces is via multiple coordination, with the most stable configuration being a cis arrangement with di-σ bonding of the C=O bond across a Cu–Cu bridge and an additional π bonding to a Pt atom. The fact that Pt significantly affects the adsorption of unsaturated aldehydes such as crotonaldehyde explains why the kinetics of their hydrogenation using single-atom alloy (SAA) catalysts vary with alloy composition, as we previously reported, and brings into question the simple model in which the role of Pt is only to promote the dissociation of H₂.

Keywords: catalysis; single-atom alloys; selective hydrogenation; unsaturated aldehydes; density functional theory



Citation: Ruvalcaba, R.; Guerrero-Sanchez, J.; Takeuchi, N.; Zaera, F. Crotonaldehyde Adsorption on Cu-Pt Surface Alloys: A Quantum Mechanics Study. *Chemistry* **2023**, *5*, 463–478. <https://doi.org/10.3390/chemistry5010034>

Academic Editors: José Antonio Odriozola, Hermenegildo García and Gianguido Ramis

Received: 27 January 2023

Revised: 23 February 2023

Accepted: 1 March 2023

Published: 3 March 2023



Copyright: © 2023 by the authors. Licensee MDPI, Basel, Switzerland. This article is an open access article distributed under the terms and conditions of the Creative Commons Attribution (CC BY) license (<https://creativecommons.org/licenses/by/4.0/>).

1. Introduction

Heterogeneous catalysis is at the center of a vast range of industrial processes, and many of the catalysts used in these are based on transition-metal nanoparticles (NPs) dispersed on high-surface-area supports [1–3]. It has long been recognized that the performance of pure metals is not always optimal and needs to be improved via the addition of other elements; alloys in particular afford the fine-tuning of the electronic properties of metals for this purpose [4–6]. Metal alloying has been a useful approach when designing selective hydrogenation catalysts, as it is often the case that platinum-group metals (Pt, Pd, and Rh in particular) are the most active promoters of hydrogenations of organic feedstocks with multiple unsaturations but are not particularly discriminating; the main product usually is the fully hydrogenated molecules [1,7–9].

In order to tame the activity of Pt, Pd, Rh, or Ir metals and to improve their selectivity, it has been customary to add a second metal as an additive [1,6,10]. Sn, for instance, has been used extensively to modify the performance of Pt-based catalysts in oil-refining processes [4,11–15]. More recently, this line of thought has been turned on its head, because when it comes to hydrogenation selectivity, it is quite possible that coinage metals may be the best choices [16–18]. Unfortunately, pure coinage metals are often not viable hydrogenation catalysts because they are not effective at promoting the required scission of the H–H bond in H₂ [17,19,20]. For that, it may be a good solution to add a platinum metal (Pt, Pd) as an additive and a minority component. Accordingly, it may be that once hydrogen atoms are produced on the Pt or Pd sites and spilled over onto the coinage metal substrate, the rest of the hydrogenation steps can take place selectively. This is the premise

underpinning the excitement over the new generation of so-called single-atom alloy (SAA) catalysts [21–24].

Much surface-science work with model systems [25,26], in conjunction with quantum mechanics calculations [27,28], has provided support for the viability of SAAs functioning according to the mechanism stated above. However, with realistic supported catalysts and in catalytic processes carried out under atmospheric conditions, a number of complications arise requiring further consideration [29]. For one, individual atoms within alloys can easily diffuse in and out of the surface of the bimetallic NPs, a process often facilitated by temperature and also by the presence of the reaction mixture [16,30–35]. It is therefore important to determine where the minority metal in SAAs is placed within the supported bimetallic NPs during the catalytic reaction. In addition, alloying one metal with another modifies its electronic properties, potentially changing its chemical behavior [36–39]. It has been recently argued that the *d* band of platinum-group and coinage metals display maximum density of states (DOS) at significantly different energies, a fact that minimizes any orbital mixing when alloying the two [27,28,39–41]; this would justify considering the minority metal (Pt, Pd) as isolated and unaffected by the surrounding majority component (Cu, Ag, Au). Nevertheless, some electron transfer is still likely to happen, and, in any case, if not the *d* orbitals, at least the *sp* band is fully delocalized across the whole bimetallic NP and can be affected by metal mixing [42]. Additional entropic factors may be introduced by the reaction mixture as well [43].

Lastly, many adsorbates require multiple-atom ensembles to bind to the surface, and new combinations of those become available in bimetallic NPs [44–46]. The added flexibility in creating new atom ensembles on the surface is in fact the basis for much catalysis design, to, for instance, minimize coke formation in reforming processes [47]. It is therefore important to understand how the addition of a second metal in SAAs may affect the adsorption energetics of the reactants [48,49]. This is the issue addressed in the present report. Our study focuses on the adsorption of crotonaldehyde, a prototypical unsaturated aldehyde, and on Cu surfaces modified by diluted Pt atoms. Cu-Pt SAAs have already been shown to improve the selectivity of several hydrocarbon conversions [33,50–53], including the hydrogenation of unsaturated aldehydes [16,54]. However, kinetic data acquired for those reactions as a function of alloy composition have suggested that the role of the added Pt is not only to promote H₂ activation, that is, to help with the dissociation of the H–H bond, but to also affect the subsequent hydrogenation of the unsaturations of the reactant, the C=C and C=O bonds in the case of unsaturated aldehydes [54]. Here, we provide results from density functional theory (DFT) calculations indicating that, indeed, the addition of Pt atoms to Cu surfaces modifies the uptake of unsaturated aldehydes, changing their adsorption geometry to favor multiple coordinations and increasing their adsorption energy. It is argued that the role of the added Pt in these SAAs is more complex than previously appreciated.

2. Methods

The quantum mechanics study reported here relied on spin-unrestricted first-principles calculations based on periodic DFT, as implemented in the Vienna Ab initio Simulation Package (VASP) [55]. The calculations were performed using the Projector Augmented Wave (PAW) pseudopotentials [56,57]. The exchange-correlation energy was described using the generalized gradient approximation with the Perdew-Burke-Ernzerhof (PBE-GGA) parameterization [58]. The electronic states were expanded in plane waves with an energy cutoff of 400 eV. Forces on individual atoms were optimized up to 1×10^3 Ry/a.u. The Van der Waals interactions were modeled using the Grimme D3 method [59]. The Brillouin zone integrations were performed using $10 \times 10 \times 10$ and $5 \times 5 \times 1$ Monkhorst-Pack k-point grids [60] for the bulk and the surfaces, respectively, and a Methfessel-Paxton smearing [61] of the second order of the Fermi-Dirac distribution function was used, with a width of 0.2 eV. The lattice parameter used for bulk Cu, which was structurally optimized, was $a = 0.36$ nm. Using the supercell method, the surfaces were modeled by periodically

repeating slabs with nine atomic planes along the [111] direction and with a vacuum larger than 10 Å. The bimetallic surfaces, the Cu₃Pt/Cu(111) and Cu₂Pt/Cu(111) systems, were constructed by adding Pt atoms in the periodic patterns shown in Figure 1a, but only on the topmost layer; all the other subsurface layers consisted of pure Cu. The structures of all these cells were optimized before exploring the adsorption of crotonaldehyde. It is worth pointing out that the size and shape of the unit cells are different in the two alloy cases, as the periodicity of the alloys is defined by their stoichiometry and fixes the characteristics of their repetitive pattern. The Hessian matrix and phonon frequencies were calculated using the finite differences method. The infrared absorption spectroscopy intensities were calculated using Density Functional Perturbation Theory (DFPT) [62] and processed using the program published by David Karhánek [63] based on linear response theory. The illustrations of the crystal structures and graphs presented in this paper were generated using the VESTA [64] and Matplotlib [65] codes, respectively.

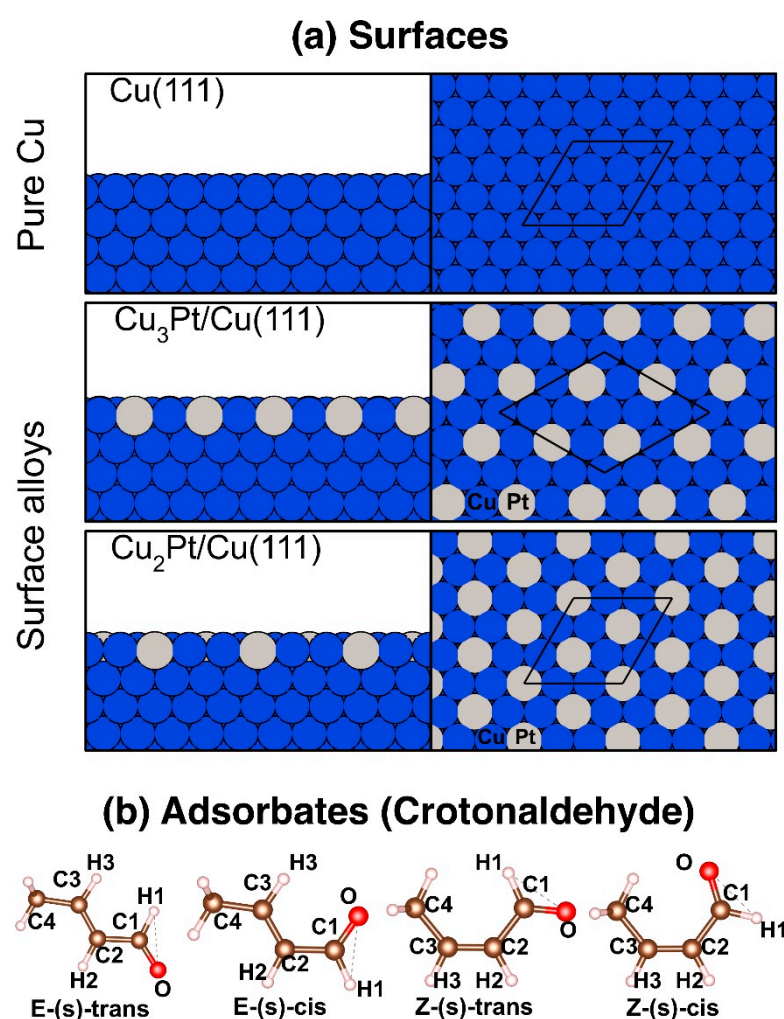


Figure 1. (a) Side (left) and top (right) views of the pristine Cu(111) and of the simulated Cu₃Pt/Cu(111) and Cu₂Pt/Cu(111) alloy surfaces used in this study. The corresponding (3 × 3), (2√3 × 2√3)R30°, and (3 × 3) supercells are shown in the top views. (b) Optimized structures for the different configurations of crotonaldehyde in the gas phase.

On the basis of our quantum mechanical calculations, adsorption energies were calculated using the following equation:

$$E_{\text{ads}} = E_{\text{surface crotonaldehyde}} - E_{\text{surface}} - E_{\text{isolated crotonaldehyde}}$$

where $E_{\text{surface crotonaldehyde}}$ reflects the energy of every adsorption configuration considered in this study, E_{surface} is the energy of the clean surface in each case (for each alloy), and $E_{\text{isolated crotonaldehyde}}$ is the energy of the isolated molecule in the gas phase. All E_{ads} is reported in units of kJ/mol.

3. Results

3.1. Energetics and Structural Properties

Calculations were first carried out for the four rotational conformers of crotonaldehyde in the gas phase: E-(s)-trans, E-(s)-cis, Z-(s)-trans, and Z-(s)-cis (Figure 1b). E-(s)-trans was found to be the most stable conformer, and the other structures to exhibit higher energies by differences of 9.6, 11.8, and 16.0 kJ/mol, respectively. In the following study, only the adsorption of crotonaldehyde in its E-(s) configurations was considered, because those are the most stable.

The bonding of crotonaldehyde to the $\text{Cu}_2\text{Pt}/\text{Cu}(111)$ and $\text{Cu}_3\text{Pt}/\text{Cu}(111)$ surfaces was optimized for both the cis and trans isomers considering a variety of coordination modes, ranging from a single coordination via the oxygen atom ($\eta^1\text{-O}$) to a fourfold coordination via bonding to all O, C_1 , C_2 , and C_3 atoms (η^4). The most stable structures obtained for each case are shown in Figure 2, and the corresponding energetics of adsorption reported in Figure 3. The adsorption energies for cis- and trans-crotonaldehydes on pure Cu(111) and Pt(111), reported before [66], were included in Figure 3 for reference. The key bond distances estimated for the adsorbed structures calculated for the cis and trans isomers are summarized in Tables 1 and 2, respectively.

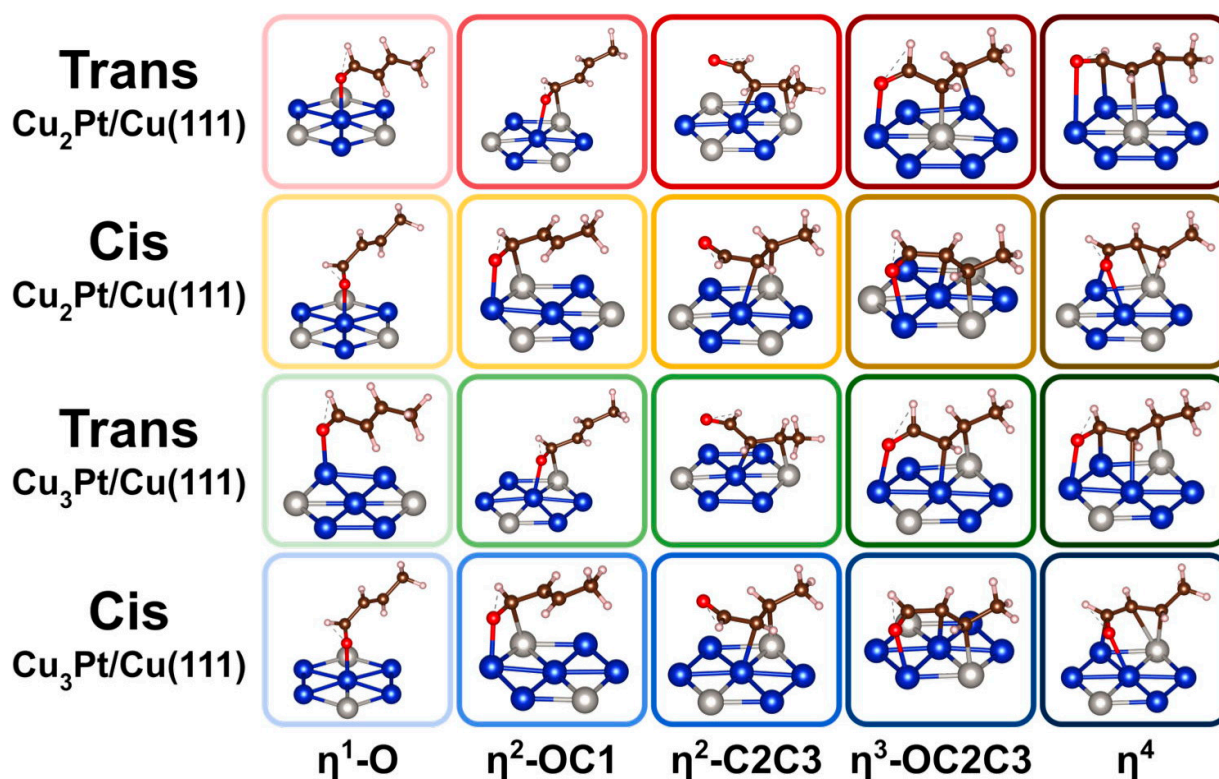


Figure 2. Optimized structures calculated for the cis and trans configurations of crotonaldehyde adsorbed on $\text{Cu}_2\text{Pt}/\text{Cu}(111)$ and $\text{Cu}_3\text{Pt}/\text{Cu}(111)$ surfaces, as a function of coordination mode. Atom color code: blue = Cu, grey = Pt, red = O, brown = C, and white (small) = H.

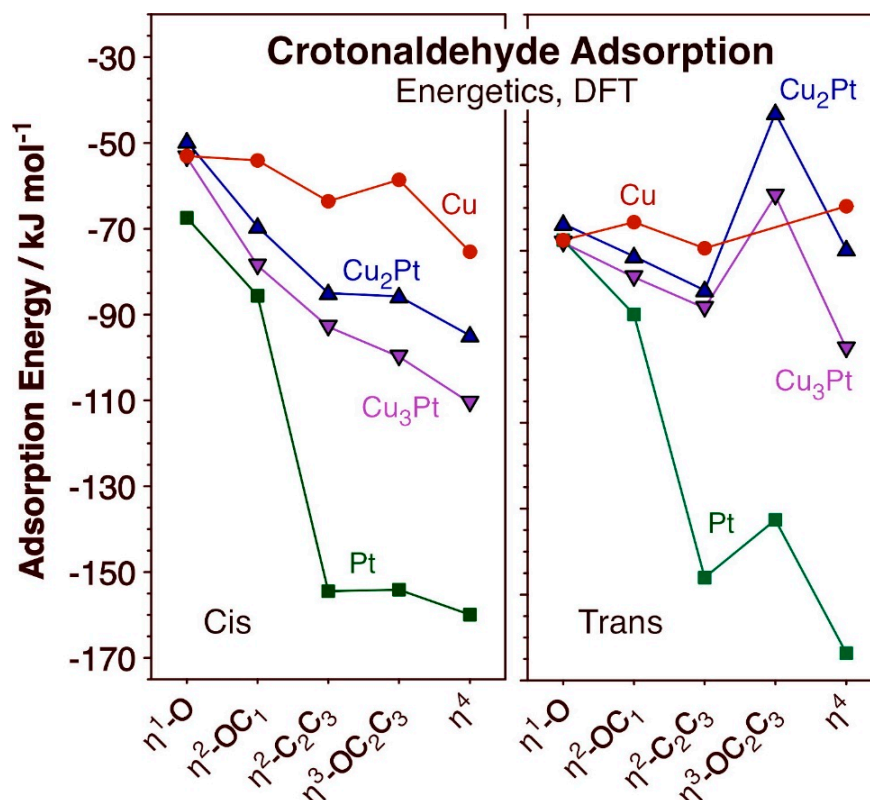


Figure 3. Energies of adsorption for the cis (left panel) and trans (right) configurations of crotonaldehyde on Cu (red circles), Cu_3Pt (pink downward-pointing triangles), Cu_2Pt (blue upward-pointing triangles), and Pt (green squares) as a function of coordination mode to the surface, for the structures shown in Figure 2.

Some interesting trends are evident from the data in Figures 2 and 3. In terms of bonding, it is seen that, in all cases, single coordination of crotonaldehyde to the surface is via the formation of a Cu–O bond. On pure Pt η^1 bonding is also via the terminal oxygen atom, but in both alloy surfaces attachment to the Cu atoms is still preferred. On the other hand, the $\eta^2\text{-OC}_1$ and $\eta^2\text{-C}_2\text{C}_3$ coordinations are the most stable if the carbon atom binds to an adjacent Pt center (the oxygen atom still binds to Cu); the latter is the most stable of the two in all four surfaces considered here. In terms of the relative behavior of the cis versus trans isomers, the former is always less stable than the latter in the low-coordination $\eta^1\text{-O}$ and $\eta^2\text{-OC}_1$ configurations, but that trend flips for the $\eta^2\text{-C}_2\text{C}_3$ case (except on pure Cu(111)); the possibility of having the C_3 atom interact with a surface Pt center provides a particularly large stabilizing effect. Then, for the $\eta^3\text{-OC}_2\text{C}_3$ and η^4 coordinations, the cis isomer is always the most stable of the two. This can be justified in terms of an increase in chain stress forced by the multiple coordination to the surface in the trans case, but it is also interesting to note that, in the structures shown in Figure 2, the C=C double bond coordinates to the surface of the alloys in a di- σ rehybridized form across a Cu–Pt bridge in the trans cases but it does so via π bonding to a single Pt atom with the cis isomer. Curiously, the same difference in bonding mode was seen on pure Cu(111) and Pt(111) surfaces [66]. It has been previously reported that the most stable form of adsorbed ethylene on both Cu(111) and $\text{Cu}_3\text{Pt}(111)$ is in the π geometry, on $\text{Cu}_3\text{Pt}(111)$ on a Pt atop site, and the vibrational spectrum of ethylene adsorbed on Cu(111) was found to be very different from that observed on $\text{Cu}_3\text{Pt}(111)$ [67]. It can be inferred that π bonding of C=C double bonds is favored over di- σ coordination, hence the stronger adsorption of the cis- (versus trans-) crotonaldehyde reported here.

Table 1. Calculated bond lengths for the E-(s)-cis crotonaldehyde in the different configurations considered in this work. Values for bonding to either Cu or Pt are indicated by the color of the numbers, blue for Cu and grey for Pt.

Geometry	Gas Phase		Cu ₂ Pt/Cu(111)				Cu ₃ Pt/Cu(111)				
	E-(s)-cis	η ¹ -O	η ² -OC ₁	η ² -C ₂ C ₃	η ³ -OC ₂ C ₃	η ⁴ -OC ₁ C ₂ C ₃	η ¹ -O	η ² -OC ₁	η ² -C ₂ C ₃	η ³ -OC ₂ C ₃	η ⁴ -OC ₁ C ₂ C ₃
Supercell	-	3 × 3	3 × 3	3 × 3	3 × 3	3 × 3	2√3 × 2√3	2√3 × 2√3	2√3 × 2√3	2√3 × 2√3	2√3 × 2√3
E _{ab} (kJ/mol)	-	-49.7	-69.57	-85.0	-85.7	-94.8	-53.3	-78.6	-92.850	-99.8	-110.5
d(C ₁ =O)	1.227	1.247	1.287	1.240	1.270	1.252	1.250	1.307	1.236	1.278	1.273
d(C ₁ -C ₂)	1.474	1.455	1.461	1.461	1.434	1.462	1.453	1.465	1.470	1.425	1.443
d(C ₂ =C ₃)	1.346	1.348	1.355	1.428	1.445	1.418	1.352	1.359	1.450	1.457	1.431
d(C ₃ -C ₄)	1.486	1.482	1.485	1.512	1.512	1.502	1.483	1.485	1.514	1.514	1.509
d(O-Cu/Pt)	-	2.304	2.101	-	2.285	2.538	2.236	2.032	-	2.149	2.258
d(C ₁ -Cu/Pt)	-	-	2.430	-	-	2.645	-	2.299	2.655	-	2.435
d(C ₂ -Cu/Pt)	-	-	-	2.416	2.277	2.277	-	-	2.226	2.212	2.456
d(C ₃ -Cu/Pt)	-	-	-	2.229	2.201	2.242	-	-	2.180	2.188	2.182

Table 2. Calculated bond lengths for the E-(s)-trans crotonaldehyde in the different configurations considered in this work. Values for bonding to either Cu or Pt are indicated by the color of the numbers, blue for Cu and grey for Pt.

Geometry	Gas Phase		Cu ₂ Pt/Cu(111)				Cu ₃ Pt/Cu(111)				
	E-(s)-trans	η ¹ -O	η ² -OC ₁	η ² -C ₂ C ₃	η ³ -OC ₂ C ₃	η ⁴ -OC ₁ C ₂ C ₃	η ¹ -O	η ² -OC ₁	η ² -C ₂ C ₃	η ³ -OC ₂ C ₃	η ⁴ -OC ₁ C ₂ C ₃
Supercell	-	3 × 3	3 × 3	3 × 3	3 × 3	3 × 3	2√3 × 2√3	2√3 × 2√3	2√3 × 2√3	2√3 × 2√3	2√3 × 2√3
E _{ab} (kJ/mol)	-	-68.7	-75.5	-84.2	-43.0	-72.8	-73.1	-81.2	-88.3	-62.2	-97.7
d(C ₁ =O)	1.226	1.247	1.262	1.240	1.270	1.252	1.242	1.296	1.237	1.243	1.275
d(C ₁ -C ₂)	1.463	1.455	1.457	1.461	1.434	1.462	1.444	1.464	1.463	1.474	1.434
d(C ₂ =C ₃)	1.346	1.348	1.353	1.428	1.445	1.418	1.349	1.359	1.446	1.466	1.440
d(C ₃ -C ₄)	1.488	1.482	1.486	1.512	1.512	1.502	1.484	1.483	1.516	1.512	1.511
d(O-Cu/Pt)	-	2.427	2.280	-	2.323	3.087	2.198	2.069	-	2.234	2.148
d(C ₁ -Cu/Pt)	-	-	2.604	-	-	2.898	-	2.330	-	-	2.550
d(C ₂ -Cu/Pt)	-	-	-	2.340	2.145	2.815	-	-	2.247	2.142	2.428
d(C ₃ -Cu/Pt)	-	-	-	2.233	2.217	2.978	-	-	2.191	2.161	2.178

Another observation deriving from the calculations reported in Figures 2 and 3 is that, in general, higher coordination to the surface stabilizes the adsorbates. This trend is more clearly seen with the cis isomer but it often applies to the trans configuration as well, the exception being the η³-OC₂C₃ bonding mode, which appears to be destabilized by the strain put on the hydrocarbon chain. As a consequence, the most stable adsorbed species in almost all cases is the one with η⁴ coordination to the surface; only with the trans isomer does a η²-C₂C₃ coordination prevail over the η⁴ option on Cu(111) and Cu₂Pt/Cu(111). It should be noted that higher coordination typically leads to a larger footprint of the adsorbates on the surface, which may be viable only at low coverages. As the coverage increases, more compressed layers form, thus destabilizing such multiple bonding. The end result is that, at times, the adsorption geometry may change to a less coordinated arrangement. In the case of acrolein on Cu(111), for instance, a switch from η⁴ to η³-OC₂C₃ was calculated when transitioning from a coverage of θ = 1/9 ML to θ = 1/4 [18].

Additional details on the nature of the bonds in the adsorbed crotonaldehyde can be extracted from the information on bond distances provided in Tables 1 and 2. For one, it is interesting to note that, in spite of the fact that most of the configurations considered here involve some bonding through the oxygen atom in the carbonyl moiety, the C₁=O bond only stretches marginally upon bonding to the surface, by less than 0.08 Å, and often by only ~0.02 Å in the η¹-O coordination. Some rehybridization of the C=O bond would be expected in that case, but the final bond lengths seen here are quite far from those

expected for C–O single bonds (1.43 Å in ethanol); the limited bond hybridization justifies the weak nature of the adsorption of the aldehyde on the Cu surfaces. Not surprisingly, larger C–O bond lengths are observed in the structures where the bond is oriented close to parallel to the surface plane (a di- σ rehybridized structure), as seen in some of the η^2 -OC₁, η^3 -OC₂C₃, and η^4 configurations. Similar arguments can be put forward for the C₂=C₃ double bond: its length is affected only when it interacts with the surface via di- σ bonding. On the other hand, the effect in the C=C bond is more pronounced than in the C=O case, as values as high as 1.46 Å can be seen (for the η^3 -OC₂C₃ configuration of the trans isomer in Cu₃Pt/Cu(111)), an elongation more than half way toward the length of a C–C single bond (1.54 Å in ethane). It should be noted that the differences seen here between the cis and trans isomers are not too significant and cannot be used to fully explain the adsorption energy differences estimated for the two isomers. What may be relevant is that the C₁–C₂ bond distance is also affected by the adsorption, becoming shorter to different extents in the several cases considered; it appears that a degree of intramolecular rehybridization may take place. An extreme of this rehybridization can be seen for trans-crotonaldehyde adsorbed on Cu₃Pt/Cu(111) in a η^4 configuration: the C₁–C₂ and C₂=C₃ bond distances calculated for that adsorbate are 1.434 and 1.440 Å, respectively, suggestive of the formation of an allylic species with a delocalized double bond.

An important conclusion from these calculations is that the presence of Pt atoms on the surface appears to provide an additional stabilizing factor leading to stronger bonding of crotonaldehyde to the surface via multiple coordination. It is particularly notable that, whereas the adsorption energies of both cis and trans isomers of crotonaldehyde remain relatively unaffected by the extent of coordination on the Cu(111) surface, larger effects are seen on the other three surfaces. As indicated above, this is due to the additional bond that appears to form between the C₃ atom and a Pt surface atom. The observed behavior is true regardless of the presence of Cu (in the alloys, compared to pure Pt(111)), or of the coordination mode of the C=C bond, di- σ with the trans isomer or π with the cis counterpart (although the effect is larger in the latter case). It can be said that, if Pt atoms are present on the surface of the Cu–Pt SAA catalysts, they are likely to affect the energetics of the hydrogenation steps during unsaturated aldehyde hydrogenation; the role of such Pt may therefore not just be that of activating the H–H bond in H₂. Our previous kinetic studies on the catalytic hydrogenation of cinnamaldehyde promoted by CuPt_x/SBA-15 catalysts had already provided indirect evidence for this additional contribution of Pt to the kinetics and thermodynamics of the hydrocarbon conversion steps [54].

One interesting quirk seen in the data in Figure 3 is that bonding of crotonaldehyde to Cu₂Pt/Cu(111) is slightly weaker than to Cu₃Pt/Cu(111), in spite of the fact that the former surface has a higher Pt coverage than the latter. However, this difference is small, and may be related to the different sizes of the unit cells used in each case (Figure 1a), which leads to slightly different surface coverages; the structure of all adsorbates, of both cis and isomers of crotonaldehyde in all η^1 -O to η^4 configurations, are almost identical in the two alloyed surfaces (Figure 2).

To further understand the nature of the bonding of crotonaldehyde to the Cu–Pt alloys, the DOS of the various molecular orbitals were calculated for the more relevant adsorption configurations. The data for the Cu₂Pt/Cu(111) surface are shown in Figure 4. Several observations are worth highlighting. For instance, the η^1 -O structure (Figure 4a) shows several peaks at negative energies from \sim –3.0 eV to –4.5 eV related to the C₂=C₃ and C–H molecular bonds, as those do not interact with the surface. On the other hand, the peak at \sim –1.5 eV is related to the C dangling bond that develops upon O attachment to the surface. Similar behavior is observed in the η^2 -OC₁ configuration (Figure 4b), in which case the dangling bond associated with the C₁ atom disappears because of its bonding to the surface. Notice that here the peaks at more negative energies, associated with the C₂=C₃ bond, remain. In the η^2 -C₂C₃ coordination (Figure 4c), the negative peaks from \sim –3.0 eV to –4.5 eV are reduced because the C₂=C₃ bond rehybridizes and because the two carbons form two new single bonds with the surface. In exchange, a new peak

consisting mainly of CH-*sp* and O-*sp* orbitals appears around the Fermi energy. A similar trend is observed in the η^3 -OC₂C₃ (Figure 4d) and η^4 (Figure 4e) species: the molecular peaks for all double bonds disappear because the molecule is fully attached to the surface. A fact to point out here is that in the η^3 -OC₂C₃ case, there are no peaks related to C₁ dangling bonds as in η^1 -O. This is probably because there is still some interaction between the C₁ atom and the surface, a fact that confirms the high affinity of Cu-Pt alloys to form highly coordinated systems. Our DOS analysis shows that, in every adsorption geometry, there is a distinctive projected density of states that evidences the formation of bonds in the corresponding molecule-surface complex.

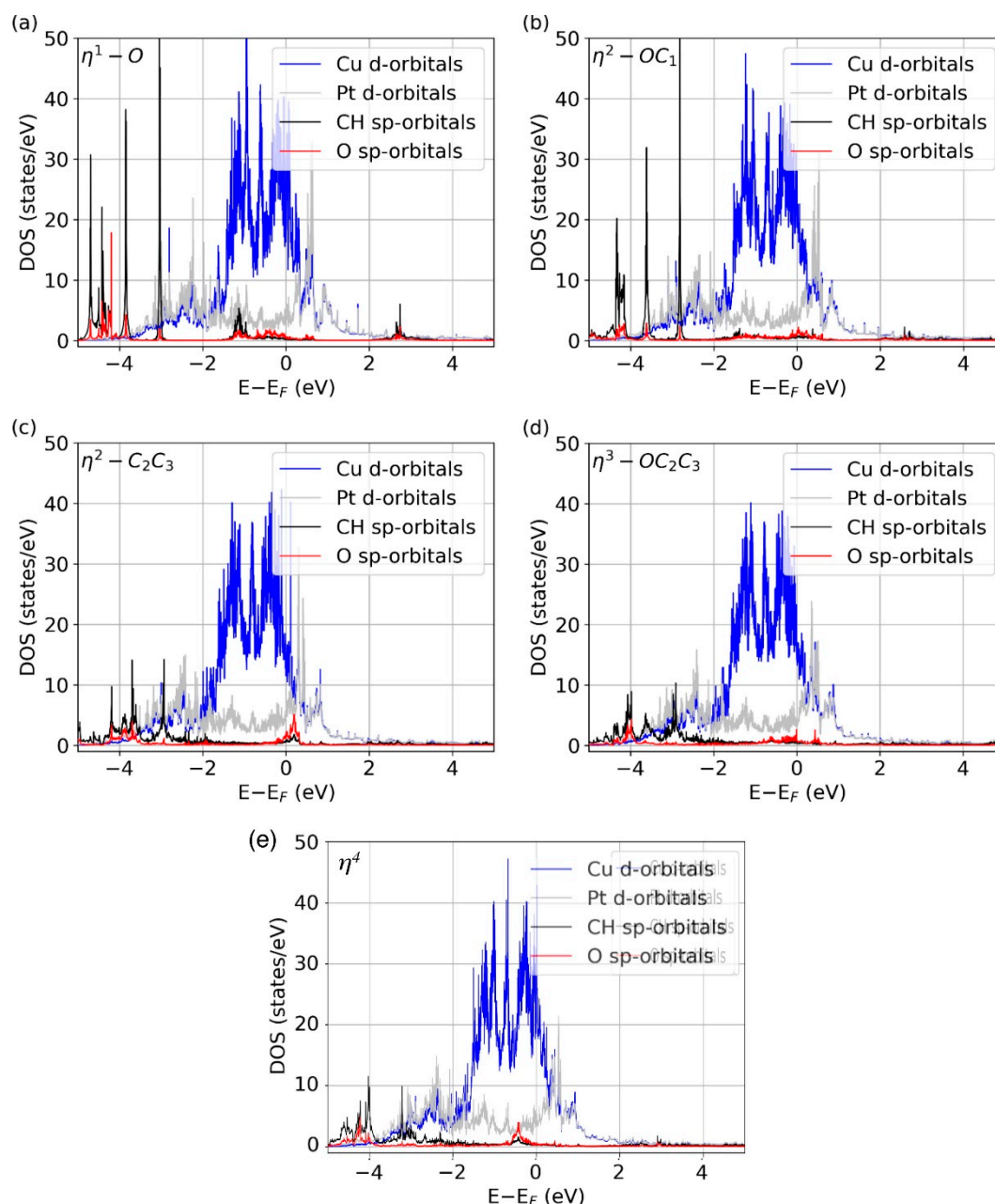


Figure 4. Projected DOS of the E-(s)-cis isomer of crotonaldehyde when adsorbed on the Cu₂Pt/Cu(111) surface in the (a) η^1 -O, (b) η^2 -OC₁, (c) η^2 -C₂C₃, (d) η^3 -OC₂C₃, and (e) η^4 adsorption configurations.

3.2. Vibrational Properties

The vibrational modes of the most stable adsorption configurations of crotonaldehyde were also calculated; they are reported in Figure 5 and in Table 3. For the Cu₃Pt/Cu(111)

surface, results are provided for the η^4 -cis, η^3 -OC₂C₃-cis, η^2 -C₂C₃-cis, and η^4 -trans configurations, whereas for the Cu₂Pt surface only the data for the η^4 -cis configuration are presented. The assignments of the modes were aided by information provided in the literature for the vibrational spectra of pure crotonaldehyde [68] as well as for crotonaldehyde adsorbed on Pt(111) [69] and on the surface of a Cu polished disk [66]. Unfortunately, there are no experimental data available in the literature for the vibrational spectra of crotonaldehyde adsorbed on Cu-Pt alloys: the IR spectra reported in our past publication with CuPt_x/SBA-15 catalysts is likely to be dominated by adsorption on the silica support (blank experiments were performed to check that; data not shown) [16], and we have not yet succeeded in preparing Pt/Cu surfaces under UHV stable enough to be useful to test the adsorption of molecules on them (as mentioned in the Introduction, us and others have determined that the Pt atoms tend to diffuse into the bulk at relatively low temperatures [16,30–35]). There are, however, high-resolution electron-loss spectroscopy data for acrolein adsorbed on Pt–Cu–Pt(111) and Cu–Pt–Pt(111) substrates (with a Cu layer in the subsurface or surface regions, respectively) [70], which can be used to extract general trends. Given the clearly distinct IR spectra obtained for crotonaldehyde on Pt(111) [69] versus polycrystalline Cu [66], the new calculations on the Cu_xPt/Cu(111) can provide some clues on what to expect in the new systems as well.

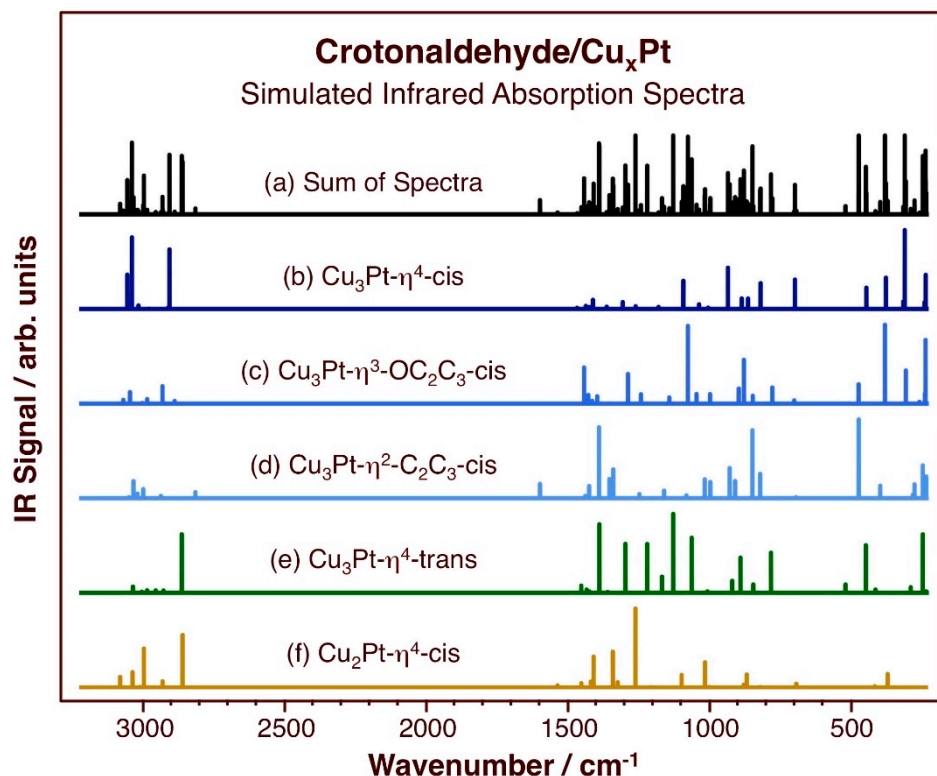


Figure 5. Calculated vibrational spectra of crotonaldehyde adsorbed on the indicated surfaces and configurations, namely, on (from top to bottom): (b) Cu₃Pt- η^4 -cis, (c) Cu₃Pt- η^3 -OC₂C₃-cis, (d) Cu₃Pt- η^2 -C₂C₃-cis, (e) Cu₃Pt- η^4 -trans, and (f) Cu₂Pt- η^4 -cis; these are the most stable adsorption structures calculated in this study. The sum of all the spectra is shown at the very top (a) as well.

One important distinctive vibrational mode in these adsorbates is the C=O stretching mode, because it appears around 1670–1710 cm⁻¹, in a range quite separate from the rest of the spectra. That mode is quite prominent in the traces for Pt(111) [69], but barely seen on Cu [66]. With acrolein, the peak is quite intense on Pt(111) (~1700 cm⁻¹) [71], but not detectable on Cu(111) [72], Cu–Pt–Pt(111), or Cu–Pt–Pt(111) [70]. Here, no peaks are seen in the spectra for adsorbed crotonaldehyde in any of the configurations for which the data were calculated. As it has been discussed before, the suggestion is that the C=O bond

may be oriented in a direction close to the plane of the surface, in which case the surface selection rule that apply to IR spectra on metals predicts no peak intensity at all [73,74]. What can be seen in the vibrational data for η^2 -C₂C₃-cis crotonaldehyde on Cu₃Pt/Cu(111) is a feature at 1594 cm⁻¹ associated with its C=C stretching mode. This is also a signature peak in the experimental data for crotonaldehyde on pure Cu (1650 cm⁻¹) [66] and for acrolein on Pt–Cu–Pt (111) (1644 cm⁻¹), but such peak is not seen with Cu–Pt–Pt(111) [70]. Overall, the relative intensities of the C=O and C=C stretching peaks can provide insightful information on the configuration adopted by unsaturated aldehydes upon adsorption; our calculations suggest that in the Cu–Pt bimetallic surfaces, they may be dominated by the features due to bonding to Cu.

Table 3. Calculated vibrational frequencies (in cm⁻¹) for the E isomers of crotonaldehyde and for the five most stable adsorption configurations *.

Geometry	Gas phase		Cu ₃ Pt/Cu(111)				Cu ₂ Pt/Cu(111)
	E-(s)-trans	E-(s)-cis	η^2 -C ₂ C ₃ -cis	η^3 -OC ₂ C ₃ -cis	η^4 -OC ₁ C ₂ C ₃ -cis	η^4 -OC ₁ C ₂ C ₃ -trans	η^4 -OC ₁ C ₂ C ₃ -cis
Supercell	-	-	$2\sqrt{3} \times 2\sqrt{3}$	$2\sqrt{3} \times 2\sqrt{3}$	$2\sqrt{3} \times 2\sqrt{3}$	$2\sqrt{3} \times 2\sqrt{3}$	3×3
ν (C–H) range	3110–2753	3095–2828	3037–2876	3045–2880	3043–2888	3022–2859	3089–2863
ν (C ₁ =O)	1701	1708					
ν (C ₂ =C ₃)	1648	1622	1594				1537
δ_a (CH ₃)				1457	1473	1456	1462
δ (CH _x)	1431, 1427	1423, 1429	1432, 1441	1423, 1435	1428, 1443	1427, 1440	1422, 1435
δ_{ip} (CH) _{ald}			1393	1400	1413	1396	
δ_s (CH ₃)	1355, 1365	1351, 1376	1348, 1356	1356	1363	1358	1334, 1358
δ_{ip} (CH) _{vinyl}	1234, 1293	1271, 1288	1265	1245, 1283	1266, 1308	1223, 1293	1201, 1268
ν (C ₁ –C ₂)	1136	1119	1148	1145	1182	1128, 1166	1110
ν (C ₃ –C ₄)	1073		1080	1049, 1080	1092	1066	
	1030	1005, 1036	1015	999	1005	1003	998, 1025
ρ (CH ₃), τ (C ₂ H ₂)	973, 996	972, 989	985		947		963
δ_{oop} (CH) _{ald}			926, 934	884, 904	823, 894	899, 920	913

* ν : stretching; δ : deformation; τ : twist; ip: in-plane; oop: out-of-plane; a: asymmetric; s: symmetric; ald: aldehyde.

The other telling region of the infrared spectra of these adsorbed species worth discussing is that between approximately 1300 and 1500 cm⁻¹, since there is where most C–H deformation modes become visible. The asymmetric deformation of the terminal methyl group in crotonaldehyde is noticeable in most spectra, on all Pt(111), Cu(111), and the mixed Pt–Cu–Pt(111) and Cu–Pt–Pt(111) surfaces; it appears at about 1450–1470 cm⁻¹ [66,70]. On the other hand, the symmetric deformation (or umbrella) mode of the methyl moiety, typically located between 1330 and 1370 cm⁻¹, has not been seen in any of those surfaces. In our calculations for crotonaldehyde on Cu_xPt/Cu(111) surfaces, several adsorption configurations do result in a detectable vibration for that mode. This is particularly noticeable for the Cu₂Pt- η^4 -cis case (1358 cm⁻¹), and to a lesser extent for the Cu₃Pt- η^3 -OC₂C₃-cis (1356 cm⁻¹) and Cu₃Pt- η^2 -C₂C₃-cis (1356 cm⁻¹) species. This pair of peaks, for the symmetric and asymmetric methyl deformation modes, can also be used to test the predictions of adsorption geometries for unsaturated aldehydes (with such methyl groups) once the experimental data become available.

4. Discussion

The main purpose of this investigation has been to assess the effect that the minority metal may play in the performance of SAA catalysts for hydrocarbon conversions. The specific case of the addition of Pt to Cu to improve on the performance of the hydrogenation of unsaturated aldehydes (crotonaldehyde) was tested by using quantum mechanics (DFT) calculations. It is often assumed that the role of Pt is only to activate molecular hydrogen and to form hydrogen atoms, which then spill over onto the Cu surface where the hydro-

carbon hydrogenation steps are expected to take place [22]. However, the adsorption of hydrocarbons often involves sites composed of ensembles of surface atom, and if single Pt atoms are present on the surface, they are likely to participate in such hydrocarbon bonding; the interaction of hydrocarbons with Pt is in general much stronger than with Cu. Our calculations, reported above, corroborate this hypothesis for the case of crotonaldehyde.

What was found in this study is that the initial bonding of unsaturated aldehydes on Cu-Pt bimetallic surfaces takes place via the carbonyl oxygen atom (Figure 2). Moreover, in a η^1 -O configuration, the molecule binds preferentially to Cu atop sites; this was previously determined to be the case on pure Cu surfaces [66], and was shown here to be true for the $\text{Cu}_2\text{Pt}/\text{Cu}(111)$ and $\text{Cu}_3\text{Pt}/\text{Cu}(111)$ surfaces as well. Similar results were also reported previously for acrolein [16,18] and for cinnamaldehyde [75]. It is somewhat surprising that on the alloys the initial bonding happens on Cu centers given that bonding to Pt is stronger, at least for the cis isomer: $E_{\text{ads}}(\eta^1\text{-O-cis, Pt}(111)) = -67.4$ kJ/mol versus $E_{\text{ads}}(\eta^1\text{-O-cis, Cu}(111)) = -53.0$ kJ/mol (Figure 3). The adsorption of the trans isomer is approximately equally strong on both metals ($E_{\text{ads}}(\eta^1\text{-O-trans, Pt}(111)) = E_{\text{ads}}(\eta^1\text{-O-trans, Cu}(111)) = -72.5$ kJ/mol), but perhaps the main reason for the preferential bonding to Cu relates to potential additional interactions of other parts of the molecule with the adjacent metal atoms present on these surfaces.

Indeed, what we found is that the presence of Pt atoms leads to a preference for multiple coordination of crotonaldehyde to the surface. On pure Cu, the adsorption energy is not very sensitive to additional interactions between any of the carbon atoms of crotonaldehyde and the surface [66], but on pure Pt, multiple coordination leads to much stronger binding [66,69], and the data reported here indicate that the same is true with the Cu-Pt alloys. For one, in all $\eta^2\text{-OC}_1$ and $\eta^2\text{-C}_2\text{C}_3$ configurations, the carbonyl and C=C groups of crotonaldehyde (respectively) both bind across a Cu–Pt bridge, with the O atoms placed on the Cu atoms and the C bonded to the Pt in the first case (Figure 2). Moreover, and more significantly, the more extensively coordinated $\eta^3\text{-OC}_2\text{C}_3$ and η^4 adsorptions show binding with both carbonyl and C=C groups, which make those species significantly more stable: the carbonyl group still binds with the O atom attached to Cu, but the C=C bond is π -bonded to a single Pt in the case of the more stable cis isomers (the trans isomer, with its weaker adsorption energies relative to the cis form, binds in a di- σ mode across a Cu–Pt bridge instead). The bottom line is that, if Pt is present on the surface of the alloy, even in single-atom form, that atom is likely to participate in the binding of the reactant, crotonaldehyde in this case. It must be concluded that, in addition to aiding in the activation of molecular hydrogen, the addition of Pt to Cu surfaces is likely to also affect the hydrocarbon hydrogenation steps. An indirect kinetic evidence for this conclusion was already obtained by us before for the case of cinnamaldehyde: both the equilibrium constants for the adsorption of the reactant and products and the reaction constants for the hydrogen incorporation steps were seen to vary with alloy composition in the $\text{CuPt}_x/\text{SBA-15}$ catalysts, some by up to three orders of magnitude [54].

The fact that single Pt atoms on Cu surfaces affect the adsorption energies of crotonaldehyde is not surprising, and is expected to be a general effect. Even with individual atoms, significant differences in adsorption energies have been calculated on ensemble sites in Cu surfaces that include one Pt atom (compared to pure-Cu ensemble sites): for instance, the addition of Pt to Cu(111) has been calculated to cause decreases in the adsorption energy of carbon, oxygen, and nitrogen atoms by approximately 14, 15, and 18 kJ/mol, respectively [28]. A possible reason for this is the small electronic contribution that the nearest Cu atoms receive from the Pt *d* orbitals, leading to a depletion of the Cu *3d* DOS. Similar effects have also been reported with other SAA metal combinations; the adsorption energy estimated for acrolein, for instance, have been shown to change upon the addition of a second dopant metal to Pt, Pd, Ni, Au, and Ag surfaces [76]. On Cu–Pt–Pt(111), where Cu is added to a Pt surface, acrolein adsorption in a η^4 configuration was estimated to

be stabilized by an additional 1.3 kJ/mol, but in the case of Pt–Cu–Pt(111), where the Cu atoms are placed on the subsurface, the adsorption is destabilized by as much as 65 kJ/mol instead [70,77]. None of these reported systems simulate SAA surfaces directly, but nevertheless point to the clear effect exerted by the addition of a second metal on adsorption energies even if they are quite diluted.

The last point to be made here is that, in these calculations, it was assumed that the minority metal, Pt, is present (in diluted form) on the surface of the SAAs. The placement of such atoms within the bimetallic nanoparticles of SAA catalysts under reaction conditions has not, however, been fully established to date. As mentioned in the introduction, both temperature and gaseous or liquid chemicals in contact with the surface of these bimetallics can induce the preferential segregation of one of the elements to the surface or its diffusion back deep into the bulk [16,30–32,34,35]. For the case of Pt added to Cu, it has been repeatedly observed that Pt often disappears from the surface, typically upon exposures to atmospheric environments but even under controlled ultrahigh vacuum (UHV) conditions. These changes are often reversible [34], which means that post-mortem analysis of the surfaces after catalysis may not reflect the nature of the active catalytic surface. It could be thought that the reactants in hydrocarbon hydrogenation reactions may in fact drive the Pt atoms to the surface, as that metal binds the reactants more strongly than Cu, but experiments with CO have shown the opposite behavior [16,34]. Clearly, our calculations here only address the situation where the Pt atoms are present on the surface; the conclusion that Pt affects the adsorption energies of the reactants and products and therefore the kinetics of the catalysis may not apply if those atoms diffuse into the bulk during reaction. Additional studies would need to be carried out to evaluate those circumstances, as Pt may still exert a remote electronic effect in those cases.

5. Conclusions

Quantum mechanics (DFT) calculations were performed to assess the details of the adsorption of crotonaldehyde on two Cu–Pt alloy surfaces, namely, on ordered Cu₂Pt/Cu(111) and Cu₃Pt/Cu(111) structures, where Pt was added only to the top-most (exposed) surface, and compared with similar estimates previously carried out by us on pure Cu(111) and pure Pt(111) [66]. Different coordination modes were considered, from single bonds, which were found to be the most stable between the O atom in the carbonyl moiety of the unsaturated aldehyde and a Cu atom in an atop position, to η^4 configurations involving the O atom together with its three nearest C atoms in the hydrocarbon chain. Both cis and trans isomers of crotonaldehyde were considered as well. From an energetics point of view, it was determined that the addition of Pt atoms to the surface, even in dilute form, increases the magnitude of the adsorption energy. Two possible η^2 binding forms were tested, via the carbonyl (OC₁) and via the C=C (C₂C₃) double bonds, and the latter was found to be the more favorable of the two in all cases. Regardless, bonding in all those structures was determined to occur in di- σ fashion, across a Cu–Pt bridge. Coordination in η^3 -OC₂C₃ mode provides additional stability for the cis isomer but not for the trans counterpart, presumably because of the chain strain required to accommodate the multiple bonding in the latter case. Finally, η^4 -OC₁C₂C₃ is the preferred coordination in most cases, except for the trans isomer on pure Cu(111) and on Cu₂Pt/Cu(111), for which the η^2 -C₂C₃ binding is slightly preferred. Ultimately, the cis isomer is more stable than the trans counterpart on all surface, in the case of the η^4 configuration apparently because the C=C double bond π coordinates to a single Pt atom (it rehybridizes to a di- σ configuration across a Cu–Pt bridge with the trans isomer). Additionally, the addition of Pt to the surface increases the magnitude of the adsorption energy of the most stable configurations by approximately 20 to 40 kJ/mol.

The stabilization of the adsorption of crotonaldehyde on the Cu–Pt alloy surfaces is also evidenced by the changes in bond distances between relevant atoms. Such changes are minor in the case of the η^1 -O coordination, where even the C₁=O bond often stretches

by less than 0.02 Å, but become more noticeable when multiple coordination is involved, especially if rehybridization to di- σ bonding occurs. In fact, with trans-crotonaldehyde, η^4 adsorption on C₃Pt/Cu(111) leads to the formation of an allylic species where the C₁–C₂ and C₂–C₃ bonds have approximately the same length. Further evidence of the stabilizing effect of Pt toward crotonaldehyde adsorption was obtained from calculations of vibrational frequencies. Although no experimental data are available yet to make full use of those results, some key pointers were nevertheless identified highlighting what to expect. On the whole, the main conclusion from our study is that, if Pt atoms are present on the surface as it has been proposed for Cu-Pt SAA catalysts, they are likely to not only help with the activation of H₂, to start hydrogenation reactions, but also affect the energetics of the subsequent H-incorporation steps into the unsaturated aldehyde hydrogenation. Past results from in situ characterization of Cu-Pt catalysts under catalytic conditions have suggested that the Pt atoms may in fact diffuse into the bulk of the bimetallic nanoparticles, in which case the results reported here would not be directly applicable, but even in that case there may be a remote electronic effect in play. This may be worth further investigation.

Author Contributions: R.R. and J.G.-S. carried out the calculations and performed the initial data analysis and interpretation. N.T. supervised the theoretical work, acquired funding for it, contributed with further data analysis, and helped with manuscript preparation. F.Z. conceived the project, acquire funding for it, directed the research, carried out the final complete data analysis, and wrote the manuscript. All authors have read and agreed to the published version of the manuscript.

Funding: This research was funded by the U.S. National Science Foundation, Division of Chemistry (NSF-CHE1953843; F.Z.) and DGAPA-UNAM (projects IN105722, IA100920), and Conacyt (A1-S-9070; R.R., J.G.-S., N.T.). Calculations were performed in the DGCTIC-UNAM Supercomputing Center, projects LANCAD-UNAM-DGTIC-051, and LANCAD-UNAM-DGTIC-368.

Data Availability Statement: Original data may be provided upon request to the authors.

Conflicts of Interest: The authors declare no conflict of interest.

References

1. Bond, G.C. *Metal-Catalysed Reactions of Hydrocarbons*; Springer: New York, NY, USA, 2005.
2. Sanfilippo, D.; Rylander, P.N. Hydrogenation and Dehydrogenation. In *Ullmann's Encyclopedia of Industrial Chemistry*; Wiley-VCH Verlag GmbH & Co. KGaA: Weinheim, Germany, 2012; Volume 18, pp. 451–471.
3. Ma, Z.; Zaera, F. Heterogeneous Catalysis by Metals. In *Encyclopedia of Inorganic and Bioinorganic Chemistry*; Scott, R.A., Ed.; John Wiley & Sons, Ltd.: Chichester, UK, 2014; p. eibc0079.
4. Sinfelt, J.H. *Bimetallic Catalysts: Discoveries, Concepts and Applications*; John Wiley and Sons: New York, NY, USA, 1983; p. 164.
5. Ferrando, R.; Jellinek, J.; Johnston, R.L. Nanoalloys: From Theory to Applications of Alloy Clusters and Nanoparticles. *Chem. Rev.* **2008**, *108*, 845–910. [[CrossRef](#)]
6. Yu, W.; Porosoff, M.D.; Chen, J.G. Review of Pt-Based Bimetallic Catalysis: From Model Surfaces to Supported Catalysts. *Chem. Rev.* **2012**, *112*, 5780–5817. [[CrossRef](#)]
7. Meemken, F.; Baiker, A. Recent Progress in Heterogeneous Asymmetric Hydrogenation of C=O and C=C Bonds on Supported Noble Metal Catalysts. *Chem. Rev.* **2017**, *117*, 11522–11569. [[CrossRef](#)]
8. Zaera, F. The Surface Chemistry of Metal-Based Hydrogenation Catalysis. *ACS Catal.* **2017**, *7*, 4947–4967. [[CrossRef](#)]
9. Zhang, L.; Zhou, M.; Wang, A.; Zhang, T. Selective Hydrogenation over Supported Metal Catalysts: From Nanoparticles to Single Atoms. *Chem. Rev.* **2020**, *120*, 683–733. [[CrossRef](#)]
10. Vilé, G.; Albani, D.; Almora-Barrios, N.; López, N.; Pérez-Ramírez, J. Advances in the Design of Nanostructured Catalysts for Selective Hydrogenation. *ChemCatChem* **2016**, *8*, 21–33. [[CrossRef](#)]
11. Burch, R.; Garla, L.C. Platinum-tin reforming catalysts: II. Activity and selectivity in hydrocarbon reactions. *J. Catal.* **1981**, *71*, 360–372. [[CrossRef](#)]
12. Joyner, R.W.; Shpiro, E.S. Alloying in platinum-based catalysts for gasoline reforming: A general structural proposal. *Catal. Lett.* **1991**, *9*, 239–243. [[CrossRef](#)]
13. Delbecq, F.; Sautet, P. Influence of Sn additives on the selectivity of hydrogenation of α - β -unsaturated aldehydes with Pt catalysts: A density functional study of molecular adsorption. *J. Catal.* **2003**, *220*, 115–126. [[CrossRef](#)]
14. Yang, X.; Koel, B.E. Adsorption and Reaction of Unsaturated Hydrocarbons on Sn/Pt Alloys. In *Encyclopedia of Interfacial Chemistry*; Wandelt, K., Ed.; Elsevier: Oxford, UK, 2018; pp. 1–10.

15. Stassi, J.; Méndez, J.; Vilella, I.; de Miguel, S.; Zgolicz, P. Synthesis of PtSn nanoparticles on carbon materials by different preparation methods for selective catalytic hydrogenation of citral. *Chem. Eng. Commun.* **2020**, *207*, 1074–1091. [[CrossRef](#)]
16. Cao, Y.; Chen, B.; Guerrero-Sánchez, J.; Lee, I.; Zhou, X.; Takeuchi, N.; Zaera, F. Controlling Selectivity in Unsaturated Aldehyde Hydrogenation Using Single-Site Alloy Catalysts. *ACS Catal.* **2019**, *9*, 9150–9157. [[CrossRef](#)]
17. Chen, B.; Zaera, F. Hydrogenation of Cinnamaldehyde on Cu(110) Single-Crystal Surfaces. *J. Phys. Chem. C* **2021**, *125*, 14709–14717. [[CrossRef](#)]
18. Nayakasinghe, M.T.; Ponce Perez, R.; Chen, B.; Takeuchi, N.; Zaera, F. Adsorption, thermal conversion, and catalytic hydrogenation of acrolein on Cu surfaces. *J. Catal.* **2022**, *414*, 257–266. [[CrossRef](#)]
19. Johansson, M.; Lytken, O.; Chorkendorff, I. The sticking probability for H₂ on some transition metals at a hydrogen pressure of 1 bar. *J. Chem. Phys.* **2008**, *128*, 034706. [[CrossRef](#)] [[PubMed](#)]
20. Álvarez-Falcón, L.; Viñes, F.; Notario-Estévez, A.; Illas, F. On the hydrogen adsorption and dissociation on Cu surfaces and nanorows. *Surf. Sci.* **2016**, *646*, 221–229. [[CrossRef](#)]
21. Han, J.; Lu, J.; Wang, M.; Wang, Y.; Wang, F. Single Atom Alloy Preparation and Applications in Heterogeneous Catalysis. *Chin. J. Chem.* **2019**, *37*, 977–988. [[CrossRef](#)]
22. Hannagan, R.T.; Giannakakis, G.; Flytzani-Stephanopoulos, M.; Sykes, E.C.H. Single-Atom Alloy Catalysis. *Chem. Rev.* **2020**, *120*, 12044–12088. [[CrossRef](#)]
23. Zaera, F. Molecular approaches to heterogeneous catalysis. *Coord. Chem. Rev.* **2021**, *448*, 214179. [[CrossRef](#)]
24. Zaera, F. Designing Sites in Heterogeneous Catalysis: Are We Reaching Selectivities Competitive with Those of Homogeneous Catalysts? *Chem. Rev.* **2022**, *122*, 8594–8757. [[CrossRef](#)]
25. Luneau, M.; Lim, J.S.; Patel, D.A.; Sykes, E.C.H.; Friend, C.M.; Sautet, P. Guidelines to Achieving High Selectivity for the Hydrogenation of α,β -Unsaturated Aldehydes with Bimetallic and Dilute Alloy Catalysts: A Review. *Chem. Rev.* **2020**, *120*, 12834–12872. [[CrossRef](#)]
26. Sykes, E.C.H.; Christopher, P. Recent advances in single-atom catalysts and single-atom alloys: Opportunities for exploring the uncharted phase space in-between. *Curr. Opin. Chem. Eng.* **2020**, *29*, 67–73. [[CrossRef](#)]
27. Thirumalai, H.; Kitchin, J.R. Investigating the Reactivity of Single Atom Alloys Using Density Functional Theory. *Top. Catal.* **2018**, *61*, 462–474. [[CrossRef](#)]
28. Schumann, J.; Bao, Y.; Hannagan, R.T.; Sykes, E.C.H.; Stamatakis, M.; Michaelides, A. Periodic Trends in Adsorption Energies around Single-Atom Alloy Active Sites. *J. Phys. Chem. Lett.* **2021**, *12*, 10060–10067. [[CrossRef](#)] [[PubMed](#)]
29. Zaera, F. In-Situ and Operando Spectroscopies for the Characterization of Catalysts and of Mechanisms of Catalytic Reactions. *J. Catal.* **2021**, *404*, 900–910. [[CrossRef](#)]
30. Zafeiratos, S.; Piccinin, S.; Teschner, D. Alloys in catalysis: Phase separation and surface segregation phenomena in response to the reactive environment. *Catal. Sci. Technol.* **2012**, *2*, 1787–1801. [[CrossRef](#)]
31. Gumuslu, G.; Kondratyuk, P.; Boes, J.R.; Morreale, B.; Miller, J.B.; Kitchin, J.R.; Gellman, A.J. Correlation of Electronic Structure with Catalytic Activity: H₂-D₂ Exchange across Cu_xPd_{1-x} Composition Space. *ACS Catal.* **2015**, *5*, 3137–3147. [[CrossRef](#)]
32. Simonovis, J.P.; Hunt, A.; Palomino, R.M.; Senanayake, S.D.; Waluyo, I. Enhanced Stability of Pt-Cu Single-Atom Alloy Catalysts: In Situ Characterization of the Pt/Cu(111) Surface in an Ambient Pressure of CO. *J. Phys. Chem. C* **2018**, *122*, 4488–4495. [[CrossRef](#)]
33. Yang, K.; Yang, B. Identification of the Active and Selective Sites over a Single Pt Atom-Alloyed Cu Catalyst for the Hydrogenation of 1,3-Butadiene: A Combined DFT and Microkinetic Modeling Study. *J. Phys. Chem. C* **2018**, *122*, 10883–10891. [[CrossRef](#)]
34. Han, T.; Li, Y.; Cao, Y.; Lee, I.; Zhou, X.; Frenkel, A.I.; Zaera, F. In situ identification of surface sites in Cu–Pt bimetallic catalysts: Gas-induced metal segregation. *J. Chem. Phys.* **2022**, *157*, 234706. [[CrossRef](#)]
35. Finzel, J.; Christopher, P. Dynamic Pt Coordination in Dilute AgPt Alloy Nanoparticle Catalysts Under Reactive Environments. *Top. Catal.* **2022**, *65*, 1587–1603. [[CrossRef](#)]
36. Rodriguez, J.A. Physical and Chemical Properties of Bimetallic Surfaces. *Surf. Sci. Rep.* **1996**, *24*, 223–287. [[CrossRef](#)]
37. Wang, Y.; Balbuena, P.B. Design of Oxygen Reduction Bimetallic Catalysts: Ab-Initio-Derived Thermodynamic Guidelines. *J. Phys. Chem. B* **2005**, *109*, 18902–18906. [[CrossRef](#)]
38. Medford, A.J.; Vojvodic, A.; Hummelshøj, J.S.; Voss, J.; Abild-Pedersen, F.; Studt, F.; Bligaard, T.; Nilsson, A.; Nørskov, J.K. From the Sabatier principle to a predictive theory of transition-metal heterogeneous catalysis. *J. Catal.* **2015**, *328*, 36–42. [[CrossRef](#)]
39. Greiner, M.T.; Jones, T.E.; Beeg, S.; Zwiener, L.; Scherzer, M.; Girgsdies, F.; Piccinin, S.; Armbrüster, M.; Knop-Gericke, A.; Schlögl, R. Free-atom-like d states in single-atom alloy catalysts. *Nat. Chem.* **2018**, *10*, 1008–1015. [[CrossRef](#)]
40. Duchesne, P.N.; Li, Z.Y.; Deming, C.P.; Fung, V.; Zhao, X.; Yuan, J.; Regier, T.; Aldalbahi, A.; Almarhoon, Z.; Chen, S.; et al. Golden single-atomic-site platinum electrocatalysts. *Nat. Mater.* **2018**, *17*, 1033–1039. [[CrossRef](#)]
41. Hopper, N.; Thuening, T.; Manzi, S.; Weinert, M.; Tysoe, W.T. Binding of Oxygen on Single-Atom Sites on Au/Pd(100) Alloys with High Gold Coverages. *J. Phys. Chem. C* **2021**, *125*, 9715–9729. [[CrossRef](#)]
42. Xin, H.; Vojvodic, A.; Voss, J.; Nørskov, J.K.; Abild-Pedersen, F. Effects of d-band shape on the surface reactivity of transition-metal alloys. *Phys. Rev. B* **2014**, *89*, 115114. [[CrossRef](#)]
43. Han, T.; Lee, I.; Cao, Y.; Zhou, X.; Zaera, F. Thermodynamics of Carbon Monoxide Adsorption on Cu/SBA-15 Catalysts: Under Vacuum versus under Atmospheric Pressures. *J. Phys. Chem. C* **2022**, *126*, 3078–3086. [[CrossRef](#)]

44. Ponec, V. Alloy catalysts: The concepts. *Appl. Catal. A* **2001**, *222*, 31–45. [[CrossRef](#)]
45. Liu, P.; Nørskov, J.K. Ligand and ensemble effects in adsorption on alloy surfaces. *Phys. Chem. Chem. Phys.* **2001**, *3*, 3814–3818. [[CrossRef](#)]
46. Gao, F.; Goodman, D.W. Pd-Au bimetallic catalysts: Understanding alloy effects from planar models and (supported) nanoparticles. *Chem. Soc. Rev.* **2012**, *41*, 8009–8020. [[CrossRef](#)] [[PubMed](#)]
47. Trimm, D.L. Coke Formation and Minimisation During Steam Reforming Reactions. *Catal. Today* **1997**, *37*, 233–238. [[CrossRef](#)]
48. Marcella, N.; Lim, J.S.; Płonka, A.M.; Yan, G.; Owen, C.J.; van der Hoeven, J.E.S.; Foucher, A.C.; Ngan, H.T.; Torrisi, S.B.; Marinkovic, N.S.; et al. Decoding reactive structures in dilute alloy catalysts. *Nat. Commun.* **2022**, *13*, 832. [[CrossRef](#)]
49. Mancera, L.A.; Diemant, T.; Groß, A.; Behm, R.J. Molecular and Dissociative Hydrogen Adsorption on Bimetallic PdAg/Pd(111) Surface Alloys: A Combined Experimental and Theoretical Study. *J. Phys. Chem. C* **2022**, *126*, 3060–3077. [[CrossRef](#)]
50. Lucci, F.R.; Liu, J.; Marcinkowski, M.D.; Yang, M.; Allard, L.F.; Flytzani-Stephanopoulos, M.; Sykes, E.C.H. Selective hydrogenation of 1,3-butadiene on platinum–copper alloys at the single-atom limit. *Nat. Commun.* **2015**, *6*, 8550. [[CrossRef](#)]
51. Humbert, M.P.; Chen, J.G. Correlating hydrogenation activity with binding energies of hydrogen and cyclohexene on M/Pt(111) (M = Fe, Co, Ni, Cu) bimetallic surfaces. *J. Catal.* **2008**, *257*, 297–306. [[CrossRef](#)]
52. Lv, C.-Q.; Liu, J.-H.; Guo, Y.; Wang, G.-C. Selective hydrogenation of 1,3-butadiene over single Pt₁/Cu(111) model catalysts: A DFT study. *Appl. Surf. Sci.* **2019**, *466*, 946–955. [[CrossRef](#)]
53. Liu, D.; Chen, H.Y.; Zhang, J.Y.; Huang, J.Y.; Li, Y.M.; Peng, Q.M. Theoretical investigation of selective hydrogenation of 1,3-butadiene on Pt doping Cu nanoparticles. *Appl. Surf. Sci.* **2018**, *456*, 59–68. [[CrossRef](#)]
54. Cao, Y.; Guerrero-Sánchez, J.; Lee, I.; Zhou, X.; Takeuchi, N.; Zaera, F. Kinetic Study of the Hydrogenation of Unsaturated Aldehydes Promoted by CuPt_x/SBA-15 Single-Atom Alloy (SAA) Catalysts. *ACS Catal.* **2020**, *10*, 3431–3443. [[CrossRef](#)]
55. Kresse, G.; Furthmüller, J. Efficient iterative schemes for ab initio total-energy calculations using a plane-wave basis set. *Phys. Rev. B* **1996**, *54*, 11169–11186. [[CrossRef](#)]
56. Blöchl, P.E. Projector augmented-wave method. *Phys. Rev. B* **1994**, *50*, 17953–17979. [[CrossRef](#)] [[PubMed](#)]
57. Kresse, G.; Joubert, D. From ultrasoft pseudopotentials to the projector augmented-wave method. *Phys. Rev. B* **1999**, *59*, 1758–1775. [[CrossRef](#)]
58. Perdew, J.P.; Burke, K.; Ernzerhof, M. Generalized Gradient Approximation Made Simple. *Phys. Rev. Lett.* **1996**, *77*, 3865–3868. [[CrossRef](#)] [[PubMed](#)]
59. Grimme, S.; Antony, J.; Ehrlich, S.; Krieg, H. A consistent and accurate ab initio parametrization of density functional dispersion correction (DFT-D) for the 94 elements H–Pu. *J. Chem. Phys.* **2010**, *132*, 154104. [[CrossRef](#)]
60. Monkhorst, H.J.; Pack, J.D. Special points for Brillouin-zone integrations. *Phys. Rev. B* **1976**, *13*, 5188–5192. [[CrossRef](#)]
61. Methfessel, M.; Paxton, A.T. High-precision sampling for Brillouin-zone integration in metals. *Phys. Rev. B* **1989**, *40*, 3616–3621. [[CrossRef](#)]
62. Wu, X.; Vanderbilt, D.; Hamann, D.R. Systematic treatment of displacements, strains, and electric fields in density-functional perturbation theory. *Phys. Rev. B* **2005**, *72*, 035105. [[CrossRef](#)]
63. Karhánek, D. *Dakarhanek/Vasp-Infrared-Intensities: Vasp-Infrared-Intensities*; (Version v1.0); Zenodo, 2020. Available online: <https://zenodo.org/record/3930989#.ZAF24R9ByUk> (accessed on 26 January 2023).
64. Momma, K.; Izumi, F. VESTA 3 for three-dimensional visualization of crystal, volumetric and morphology data. *J. Appl. Crystallogr.* **2011**, *44*, 1272–1276. [[CrossRef](#)]
65. Hunter, J.D. Matplotlib: A 2D Graphics Environment. *Comput. Sci. Eng.* **2007**, *9*, 90–95. [[CrossRef](#)]
66. Nayakasinghe, M.T.; Guerrero-Sánchez, J.; Takeuchi, N.; Zaera, F. Adsorption of crotonaldehyde on metal surfaces: Cu vs Pt. *J. Chem. Phys.* **2021**, *154*, 104701. [[CrossRef](#)]
67. Haubrich, J.; Becker, C.; Wandelt, K. Adsorption and interaction energy of π ethene on Pt(111) and Pt alloys: A detailed analysis of vibrational, energetic and electronic properties. *Surf. Sci.* **2009**, *603*, 1476–1485. [[CrossRef](#)]
68. Lindenmaier, R.; Williams, S.D.; Sams, R.L.; Johnson, T.J. Quantitative Infrared Absorption Spectra and Vibrational Assignments of Crotonaldehyde and Methyl Vinyl Ketone Using Gas-Phase Mid-Infrared, Far-Infrared, and Liquid Raman Spectra: S-cis vs s-trans Composition Confirmed via Temperature Studies and ab Initio Methods. *J. Phys. Chem. A* **2017**, *121*, 1195–1212. [[CrossRef](#)]
69. de Jesús, J.C.; Zaera, F. Adsorption and Thermal Chemistry of Acrolein and Crotonaldehyde on Pt(111) Surfaces. *Surf. Sci.* **1999**, *430*, 99–115. [[CrossRef](#)]
70. Murillo, L.E.; Menning, C.A.; Chen, J.G. Trend in the CC and CO bond hydrogenation of acrolein on Pt–M (M = Ni, Co, Cu) bimetallic surfaces. *J. Catal.* **2009**, *268*, 335–342. [[CrossRef](#)]
71. de Jesús, J.C.; Zaera, F. Double-Bond Activation in Unsaturated Aldehydes: Conversion of Acrolein to Propene and Ketene on Pt(111) Surfaces. *J. Mol. Catal. A Chem.* **1999**, *138*, 237–240. [[CrossRef](#)]
72. Islam, A.; Molina, D.L.; Trenary, M. Adsorption of acrolein and its hydrogenation products on Cu(111). *Phys. Chem. Chem. Phys.* **2022**, *24*, 24383–24393. [[CrossRef](#)] [[PubMed](#)]
73. Greenler, R.G. Infrared Study of Adsorbed Molecules on Metal Surfaces by Reflection Techniques. *J. Chem. Phys.* **1966**, *44*, 310–315. [[CrossRef](#)]

74. Zaera, F. New advances in the use of infrared absorption spectroscopy for the characterization of heterogeneous catalytic reactions. *Chem. Soc. Rev.* **2014**, *43*, 7624–7663. [[CrossRef](#)]
75. Chen, B.; Ponce, R.; Guerrero-Sánchez, J.; Takeuchi, N.; Zaera, F. Cinnamaldehyde adsorption and thermal decomposition on copper surfaces. *J. Vac. Sci. Technol. A* **2021**, *39*, 053205. [[CrossRef](#)]
76. Lucci, F.R.; Darby, M.T.; Mattera, M.F.G.; Ivimey, C.J.; Therrien, A.J.; Michaelides, A.; Stamatakis, M.; Sykes, E.C.H. Controlling Hydrogen Activation, Spillover, and Desorption with Pd–Au Single-Atom Alloys. *J. Phys. Chem. Lett.* **2016**, *7*, 480–485. [[CrossRef](#)]
77. Fan, T.; Sun, M.; Ji, Y. First-principles study on the selective hydrogenation of the C=O and C=C bonds of acrolein on Pt–M–Pt (M = Pt, Cu, Ni, Co) surfaces. *Phys. Chem. Chem. Phys.* **2020**, *22*, 14645–14650. [[CrossRef](#)] [[PubMed](#)]

Disclaimer/Publisher’s Note: The statements, opinions and data contained in all publications are solely those of the individual author(s) and contributor(s) and not of MDPI and/or the editor(s). MDPI and/or the editor(s) disclaim responsibility for any injury to people or property resulting from any ideas, methods, instructions or products referred to in the content.